A Fission-Fragment Stabilized MHD Nuclear Thermal Rocket Concept

Author(s): D. W. Cott

Session Name: Advanced Systems

SEAM: 31 (1993)

SEAM EDX URL: https://edx.netl.doe.gov/dataset/seam-31

EDX Paper ID: 1620

A FISSION-FRAGMENT STABILIZED MHD NUCLEAR THERMAL ROCKET CONCEPT[1]

by
Donald W. Cott[2]
Blue Sky Research, Inc.
Idaho Falls, Idaho

ABSTRACT

The objective of this effort was to determine how much performance improvement can be obtained from adding an MHD accelerator and auxiliary equipment to a nuclear thermal rocket. The justification for considering the concept is that it promises higher specific impulse than nuclear thermal rockets, with lower specific mass and less complication than with most nuclear electric propulsion systems. The concept is described. Key technical issues are addressed. A system level computer code for preliminary performance assessment is discussed. Performance data and parametric sweeps are presented as computed from the code. Suggestions for future work are make to investigate several remaining key technical issues.

CONCEPT DESCRIPTION

This work builds on previous work by Cott[1] including a toroidal panel magnet model that allows estimates of thrust-to-weight ratio for the first time. Parametric sweeps of specific impulse and thrust-to-weight ratio are presented for ranges of assumed maximum fuel element temperatures, maximum pressures, and neutron flux. Comparison curves are also presented for nuclear thermal rockets under the same conditions but without MHD enhancement.

As illustrated in Figure 1, the concept utilizes a liquid hydrogen propellant. The hydrogen is pumped to high pressure, then heated in a warm loop nuclear reactor pass, to the maximum temperature compatible with a rotating turbine or centrifugal expander. The flow is expanded to an intermediate pressure, spinning a shaft on which the pump and a rotating direct-current generator are attached. The electric power from the generator is bussed to an MHD accelerator, where kinetic energy is electromagnetically imparted to the nozzle flow in an annular volume around the reactor. The flow leaving the expander is injected with an alkali metal seed on entering the hot loop of the reactor, where it is heated to the maximum temperature reliably permitted by gas-cooled solid-core nuclear reactor technology. Then the flow passes through the MHD accelerator where it absorbs a significant increase in kinetic energy at about constant temperature and pressure. The flow is then expanded through a spike nozzle to the maximum practical velocity.

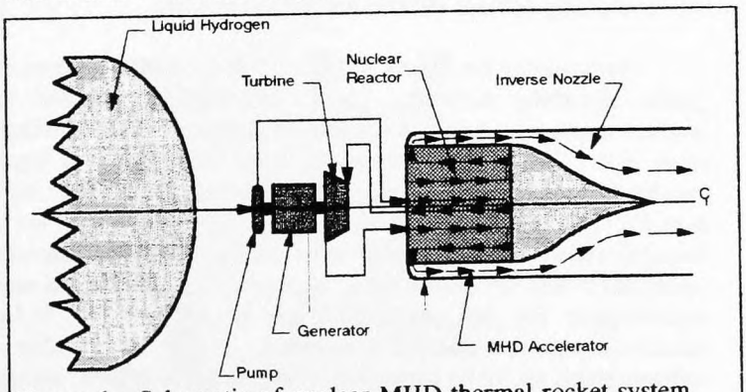

Figure 1. Schematic of nuclear MHD thermal rocket system.

The internal field relationships in the MHD accelerator are illustrated in Figure 2. Interestingly enough, this is the same basic thruster geometry as was previously introduced for submarine propulsion[2]. Ideally the reactor is a right circular cylinder, which is electrically biased such that the reactor surface serves as the MHD accelerator cathode. The outer casing is electrically isolated from the reactor and back plate, such that it can serve as the MHD accelerator anode. The two-terminal rotating generator output is applied across the annular gap between the casing and the reactor. Thus electric current density J_r flows radially inward in response to the applied radial electric field E_r. Meanwhile magnet coils to be

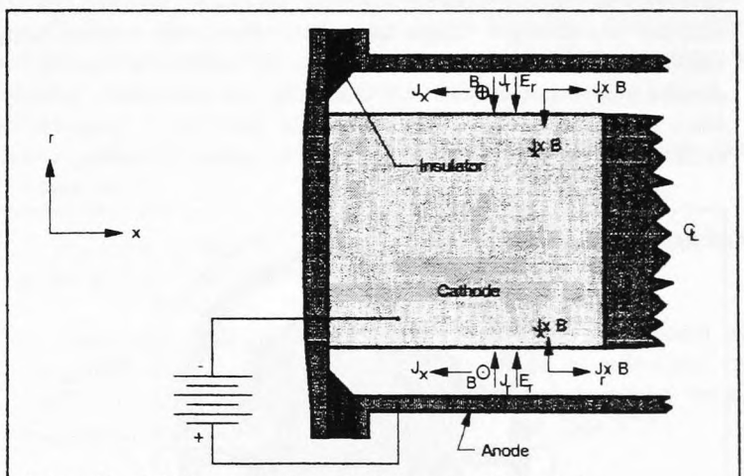

Figure 2. MHD accelerator field vector relationship.

[1]31st Symposium on Engineering Aspects of Magnetohydrodynamics, June 29-July 1, 1993.

[2]Staff Scientist, Blue Sky Research, Inc., P.O. Box 2501, Idaho Falls, ID 93403-2501, (208) 523-8285.

described later induce a tangential magnetic field B, around the annulus. The interaction of the radial current density and the tangential magnetic field induce a J,xB body force in the downstream axial direction. It is this body force that provides the primary acceleration to the flow in the annulus.

A key point to this concept is that the MHD accelerator must be wrapped very tightly around the reactor. This is required for plasma stabilization in order to operate at high power density, as will be discussed later. The major problem with this tight integration of MHD accelerator and reactor is that superconducting magnet coils must operate with an inside leg in the immediate vicinity of the reactor core, as illustrated in Figure 3 for the cylindrical configuration.

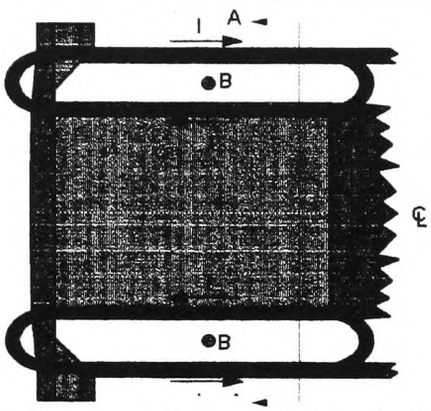

Figure 3. Superconducting magnet panel coil side view.

In Figure 3 two of the superconducting pancake magnet coils are shown in a side view. Examination of the indicated coil current shows that a fairly uniform, steady, tangential magnetic field is induced as shown in Figure 2. Section A-A of Figure 3 is illustrated in Figure 4, where slots into which the pancake coils are inserted are shown. These slots keep the annulus from being continuous around the reactor, requiring the MHD accelerator to be divided into several sectors. Only three or four coils can be utilized, since the same thickness of Dewar and shielding is required for each. Thus the toroidal magnetic field is actually a bumpy toroid,

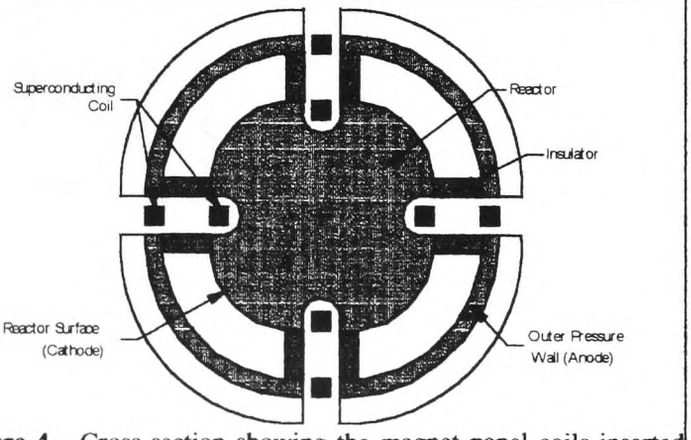

Figure 4. Cross-section showing the magnet panel coils inserted into slots in the MHD accelerator.

rather than the smooth right-circular cylinder of the more idealized Figure 2. The reactor and casing surfaces should be contoured to follow this shape to avoid eddy-current losses in the accelerator. Thus axial symmetry is lost and the construction becomes more complex.

Figure 5 shows more detail in the most sensitive part of the design. For this study it was assumed that a very advanced superconducting matrix would be utilized, but still liquid helium temperatures are required to handle the required current density. Thus the Dewar utilizes a liquid helium forced-flow around the conductor, surrounded by an annular vacuum gap containing IR radiation shields, surrounded by an annular liquid hydrogen layer. This outer hydrogen layer of the Dewar is simply the first full-flow hydrogen pass through the reactor, following first-stage pumping of the hydrogen to an adequate supply pressure for the high-pressure pump stages. Thus no attempt is made to insulate the hydrogen layer from the reactor temperature on the hot side. A separate refrigeration system is utilized to maintain the low helium temperature, rejecting heat to the liquid hydrogen between pump stages. No radiant heat rejection surfaces are required for any part of this system, this is perhaps the major advantage of this system

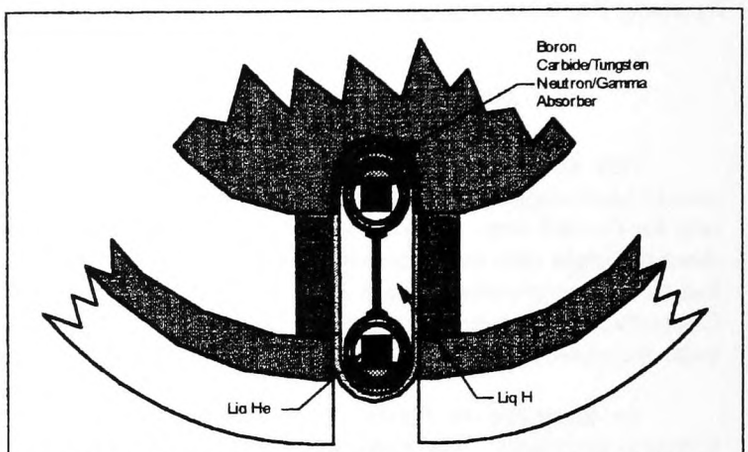

Figure 5. Superconducting coil Dewar and radiation shielding.

over competing nuclear electric propulsion systems.

Surrounding the Dewar of Figure 5 is a shield of neutron and gamma absorbing material. Ideally this shield is metallic and supplies structural support to the coils to keep them from moving to either side. The force between the inner and outer coil legs is handled by a tension web inside the liquid hydrogen Dewar layer. Radial force is greater against the inner than the outer leg, so the net force is radially inward, and must be supported by structure embedded within the reactor core. Superconducting materials under consideration for this application are Nb_3Al and $Nb_3(Al,Ge)$. Aluminum stabilizer material is assumed. Tensile force within the support panels are to be supported by boron nitride fibers, utilizing B^{11} only, in an aluminum matrix.

As the forgoing considerations illustrate, there are major engineering and physics issues involved in building and operating superconducting magnet coils adjacent to an operating nuclear reactor. The reason for wrapping the MHD accelerator so closely around the reactor is that this allows the escaping neutron flux to be used for direct ionization of the plasma. Moderately high ionization

levels are necessary in the plasma to provide an adequately high and uniform electrical conductivity. Solid core nuclear reactors are unable to provide high enough temperature for adequate thermal ionization of seeded hydrogen, except at very low pressures. This low pressure region is the traditional area within which MHD thrusters operate, but for an MHD thruster to be a practical compliment to a nuclear thermal rocket, much higher pressure operation is required.

Central to the MHD instability is electron thermal and ionizational nonequilibrium. The MHD accelerator can be run in a highly nonequilibrium mode, where the electron energy distribution is Maxwellian about an electron temperature that is significantly elevated above the heavy gas temperature. The hydrogen translational, rotational, and vibrational temperatures, and the seed ion and neutral translational temperatures, tend to be Maxwellian about the same heavy gas temperature. Thermal ionization, and hence electrical conductivity and current density, is very sensitive to the electron gas temperature. Thus when high power density operation is attempted with an MHD accelerator at high pressures, any region of slightly higher ionization than another region will draw somewhat more current. Since the local power dissipation to the electron gas component is proportional to J^2/σ, the electron temperature increases in this area of increased current density. Hence the current density increases further, and the device breaks down in a discharge across the annulus. The details of this physical model as applied to a diatomic nitrogen accelerator have been presented elsewhere by Cott[3]. Operation in this unstable regime is characterized by high anode erosion and low efficiency.

The approach used here to stabilize MHD accelerator operation at high power density and pressure is to utilize the neutron and beta flux leakage from the reactor, much as analyzed by Watanabe, et al.[4] for potassium-seeded helium-3 plasmas in MHD generators. The MHD accelerator walls are coated with ^{10}B as shown in Figure 6. ^{10}B has a very large cross section for alpha emission with thermal neutrons. The alpha particles come off at high energy and have a high ionization cross section for all the plasma components. Thus the plasma ionization is increased in a way that is not dependent on electric current density. The major question is of course whether the stabilizing effect of this neutron pumped ionization is adequate to allow stable operation of the MHD accelerator within an envelope of practical interest. While it may be acceptable to inject ^{10}B into the hydrogen as a seed, it must be insured that no boron gets into the reactor itself where it would poison the reaction. A much lesser ionization effect should be available from the reactor beta flux. Since the reactor serves as the cathode, this beta flux will augment the electron thermal emission from the reactor surface. Additionally, the beta particles are of high enough energy and cross section to increase the ionization of other species through collisions.

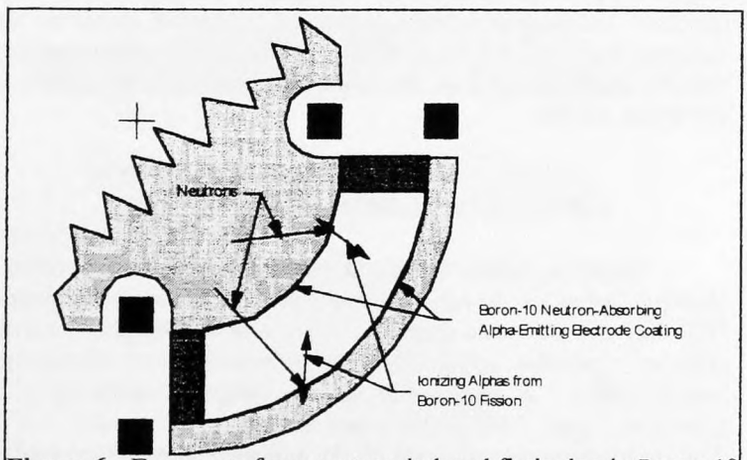

Figure 6. Fragments from neutron-induced fissioning in Boron-10 on the electrode wall coatings utilized for stabilizing ionization of the seeded hydrogen plasma in an annular accelerator.

KEY ISSUES

Several issues key to the feasibility of this concept have been touched on above. In order of importance, they can be repeated as follows:

1. Assuming the concept can be made to work, is the performance improvement worthwhile?

2. Can the MHD accelerator be radiation stabilized to work reliably at the relatively high pressure and power density required?

3. Can a magnet/dewar/shielding system be developed for this temperature/radiation environment, that will work reliably in the superconducting mode at a useful current density?

The remainder of this paper addresses the above issues.

SYSTEM MODEL

In performing a system level feasibility analysis of this concept, the primary questions to be answered are: 1) How much specific impulse improvement is attainable with this system over that of a conventional nuclear thermal rocket (NTR) system? 2) How much higher specific mass does this system have than a comparable NTR system? As a first approach to answering these questions a system model has been developed.

The following simplifying assumptions are built into the system model:

1. The working fluid is hydrogen, seeded with 1 mole% potassium in the MHD accelerator.

2. Thermodynamic properties below 1500 K are as tabulated by Vargaftik[5]. Above 1500 K the properties are as calculated by CECTRN, a locally modified computer program based on recent versions of the NASA Lewis codes CEC76[6] and TRAN72[7].

3. All the nonequilibrium phenomena are lumped together and represented simply by a multiplier on the electron number density and electrical conductivity.

4. The MHD accelerator is a continuous-wall Faraday device, with the load factor, input power, length-to-diameter ratio, and aspect ratio specified, and contoured such that the plasma static thermodynamic state is constant throughout the accelerator.

5. Viscous shear and heat losses are neglected throughout.

6. Boundary layer voltage drop is assumed negligible due to the high radiation-caused ionization near the electrode walls.

7. Each component is represented as a single node.

The code and derivations of the underlying equations are available and can be obtained from the author on request.

MAGNET MODEL

While the above described system code was developed specifically for this effort, resources were inadequate to develop a fully-comprehensive system model from scratch. Therefore the magnet model was adapted from an existing model originally developed for submarine thrusters[2]. This toroidal magnet design code was developed in MathCAD™, while the overall system code was written in FORTRAN. Thus the two codes are not fully interactive. The direction of information flow is from the system model to the magnet design code, thus the system model runs without detailed knowledge of the physical configuration of the magnet coils and support structure. This would introduce significant error in the modeling of the reactor neutronics, but has little effect at the present level of sophistication, since reactor neutronics are not yet included in the system model.

The system code insures that a successful neutronic/thermal design can be performed by allowing an adequate amount of volume for the fuel elements and flow passages, based on existing nuclear thermal rocket designs. In all cases the reactor length and diameter are kept equal. No provision is made at this stage for reactivity control, although the presence of the boron-10 coatings around the perimeter will certainly impact how control is effected. Adequate volume is provided for internal control rod insertion in the outer (low pressure) part of the core. Manifold sealing problems would make this difficult in the internal (high pressure) portion of the core.

Magnet design current density data are taken from Schwartz, et al.[8] This design data is somewhat in advance of the present state-of-the-art, but that is believed to be appropriate for a device that is unlikely to be built for several decades. The superconductor was taken to be $Nb_3Al_{0.75}Ge_{0.25}$ with a working current density between 0 and 30 T at liquid helium temperature given by

$$J_{sc} = \frac{\left[1 - \frac{B}{46T}\right]^2}{\sqrt{\frac{B}{T}}} 10^{10} \frac{A}{m^2} \qquad (1)$$

where J_{sc} is the current density, B is the magnetic field intensity, and T, A, and m are the units Tesla, Amps, and meters, respectively. Aluminum was chosen as the stabilizer. Also from Reference 8, the maximum recommended aluminum stabilizer current density for a safe quench is

$$J_{sta} = 100\ MA/m^2 \qquad (2)$$

Within the coil the area ratio of forced liquid helium coolant passage to total area is assumed to be 0.25. The structural material of the panel supporting the coil is silicon carbide, with a working stress of 1.5 GPa. The SiC is embedded in a matrix of aluminum to distribute the stress among the fibers, with a fiber to aluminum matrix ratio of 0.9. The number of amp*turns (NI_{tot}) required to produce a nominal magnetic field intensity of B_0 is

$$NI_{tot} = \frac{2\pi r_0 B_0}{\mu_0} \qquad (3)$$

from pg. 119 of Thome and Tarrh[9], where r_0 is the nominal radius from the magnet axis, and μ_0 is the magnetic permeability. From the same reference the magnetic field B for the inside and outside leg can be evaluated as

$$B = B_0 \frac{r_0}{r} \qquad (4)$$

where r is the radius of either the inside or the outside leg. The radial force per unit length on the inner and outer legs of each coil is given by

$$F = \frac{NI_{tot} B}{N_{coils}} \qquad (5)$$

where N_{coils} is the number of panel coils making up the magnet. The outer leg and end loops of the coils are supported by the panel in tension, while the inward radial force on the inside leg is supported by an aluminum bucking block inside the core. The interior of the bucking block is a rounded triangular or square cylinder, depending on whether the design uses three or four panel coils. This interior portion of the bucking block also forms the pressure wall separating the high pressure interior of the core from the low pressure, high temperature outer portion of the reactor. Short radial supports extend from the corners of the internal bucking block to support the inner legs of the coils. The bucking block wall thickness is calculated using the inner leg support force from Equation (5), using a maximum compressive working stress of 275 MPa. None of the magnet forces bear directly on the reactor fuel elements. The necessary structure to support asymmetric tangential forces on the coils are neglected for the present, but presumably this capability will be incorporated into the electrode walls as the model is developed further.

REFERENCE DESIGN PERFORMANCE

Using the system model and magnet design models described above, a reference design was developed for the overall system. Note that this reference design is in no way optimized. It serves only as a starting point for parametric studies of the system characteristics. A temperature-entropy diagram of the cycle is plotted in Figure 7 for the reference design.

The pressure-volume diagram of the reference design is similarly plotted in Figure 8. Note in Figure 7 and Figure 8 that the MHD accelerator is represented by a single point, since it operates at a constant thermodynamic static state. The specific volume change in the pumping process is fairly small, and that the pressure drop in both passes of the reactor is neglected. Neglecting this pressure drop shouldn't make any major difference in the results obtained, since increasing the supply pressure delivered by the pump is

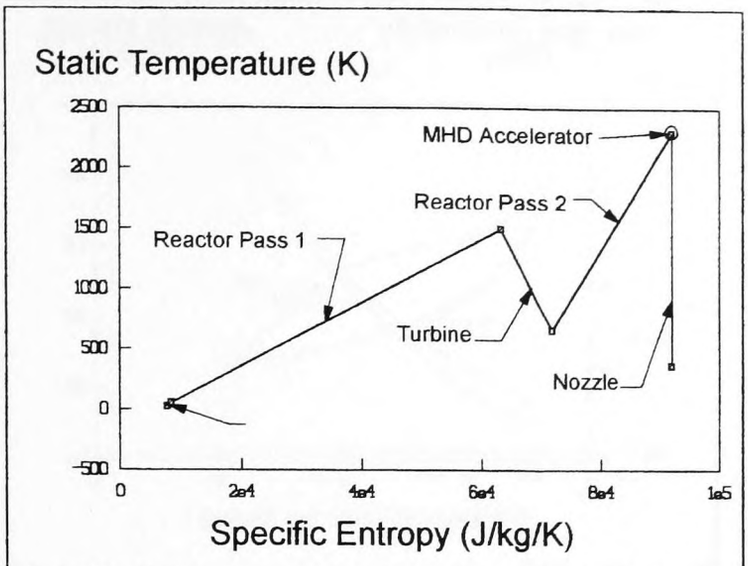

Figure 7. Temperature-entropy diagram for the reference design.

relatively inexpensive.

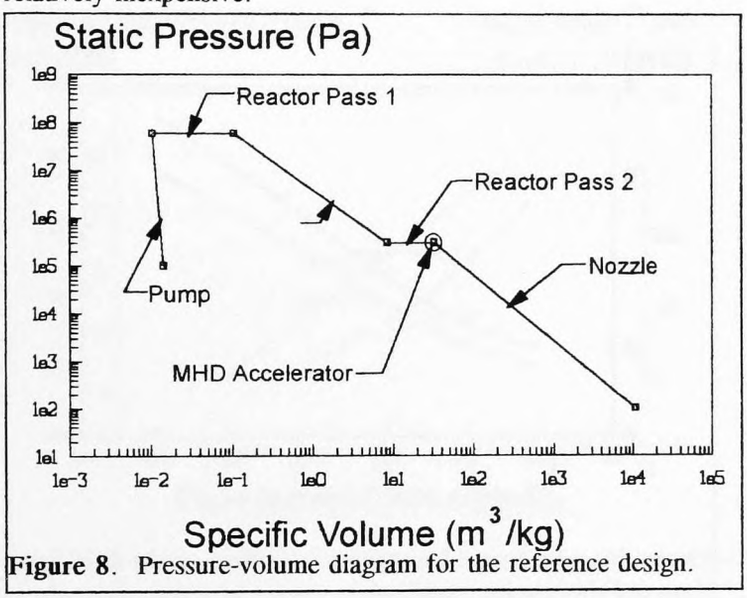

Figure 8. Pressure-volume diagram for the reference design.

Data for the Reference Design are as follows:

System Model Inputs:
Hydrogen Tank Pressure = 1 Bar
Hydrogen Tank Temperature = 20 K
Maximum Cycle Pressure = 600 Bar
Maximum Cycle Temperature = 2300 K
Nozzle Exhaust Pressure = 100 Pa
Flow Rate = 1 kg/s
Chamber Pressure = 3 Bar
Pump Efficiency = 0.9
Turbine Efficiency = 0.8
Turbine Inlet Temperature = 1500 K
MHD Load Factor = 2
Magnetic Field = 5 T
MHD Accelerator Length = 0.75 m
MHD Aspect Ratio = 0.1
Nonequilibrium Multiplier = 15

System Model Outputs:
Pump Power = 1.07 MWe
Pass 1 Heat Transfer = 21.7 MWt
Turbine Power = 13.0 MWe
Pass 2 Heat Transfer = 27.0 MWt
MHD Power Input = 11.9 MWe
MHD Output Velocity = 4880 m/s
Nozzle Output Velocity = 9290 m/s
Thrust = 9400 N
Specific Impulse = 9400 N s / kg = 959 lbf s / lbm
MHD Efficiency = 0.5
MHD Enthalpy Added = 0.33
MHD Electrical Conductivity = 16.7 S/m
Electron Number Density = 3.0e+20 / m^3
Length-to-Diameter Ratio = 3.33
Avg Width between Insulator Walls = 0.713 m
Avg Height between Electrodes = 7.13 cm
Transverse Electric Field = 12.3 KV/m
Axial Electric Field = 0
Transverse Current Density = 2540 A/m^2
Axial Current Density = -4430 A/m^2
Hall Parameter = 1.75
Push Power Density = 4.1 GW/m^3

Magnet Model Inputs:
(Selected information from system model, plus)
Number of Coils = 3

Magnet Model Outputs:
Inner Leg Magnetic Field = 5.46 T
Outer Leg Magnetic Field = 4.58 T
Total MegAmp*Turns = 10.2 MA*Turns
Nominal Superconductor Current Density = 3550 MA/m^2
Nominal Superconductor Area per Coil = 9.60 cm^2
Stabilizer Area per coil = 341 cm^2
Coolant Area per Coil = 87.6 cm^2
Total Coil Cross-sectional Area = 438 cm^2
Panel Matrix Web Thickness = 3.96 cm
Bucking Block Fin Thickness = 6.76 cm
Total Superconductor Mass = 40.5 kg
Total Stabilizer Mass = 454 kg
Total Panel Fiber Mass = 10.2 kg
Total Panel Aluminum Mass = 8.12 kg
Total Bucking Block Aluminum Mass = 154 kg
Total Magnet Mass = 666 kg
Bare-Bones NTR Mass = 725 kg

Note that this is by no means an optimized design. It is offered for the purpose of presenting a self-consistent solution of the relevant equations. Note that the specific impulse is approximately 150 s above that calculated by Parsley, et al[10], for a similar chamber condition. The code was run without the MHD accelerator for the same condition, and the resulting specific impulse was 820 s. This compares to 812 s from Reference 10, which serves as an external check on the accuracy of the code.

The bare-bones nuclear thermal rocket (NTR) mass was estimated by taking the mass and flow rate of a small NTR from Reference 10, and similar data from a large NTR reported by Clark, et al.[11], and assuming a linear variation of rocket mass to rocket flow rate. This gives a feeling for how much the magnet

mass impacts the overall mass of the rocket. It turns out for the small rocket picked for the reference design, that the magnet mass approximately doubles the rocket mass.

This gives some idea of the performance increase available from an unoptimized design. An appreciation of the complexity of the design trades can be realized by considering the parametric sweeps in the next section.

PARAMETRIC SWEEPS

Figure 9 shows the effect of increasing the maximum cycle temperature on electrical conductivity and specific impulse. The specific impulse effect is much as would be expected without the MHD accelerator, except that the curve is moved about 150 s higher. For an accelerator the electrical conductivity is in a very practical range.

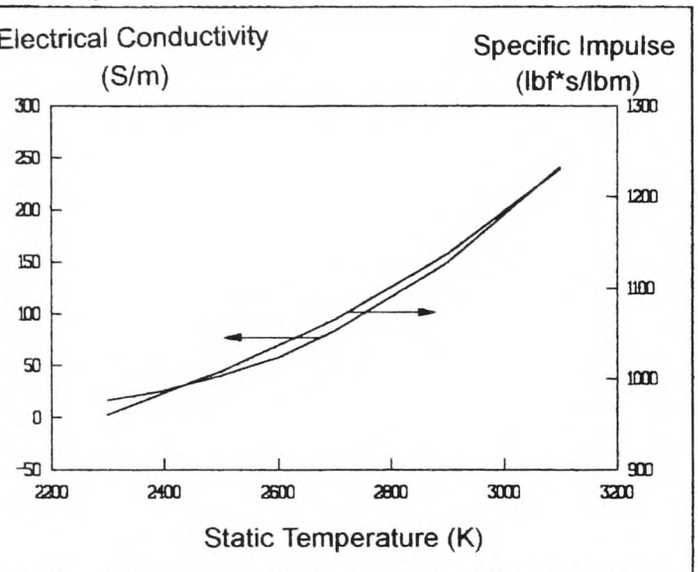

Figure 9. Maximum cycle temperature effect on electrical conductivity and specific impulse.

Figure 10 shows the effect of varying chamber pressure on electrical conductivity and specific impulse. Since this is the pressure at which the MHD accelerator operates, the effect is significant on electrical conductivity. Specific impulse is less effected, since it is primarily a function of power input to the accelerator. That power input is changed somewhat due to the changing backpressure on the turbine.

From Figure 11 it is evident that inlet temperature to the turbine has a strong effect on MHD power, and hence on specific impulse.

Figure 12 shows exactly the opposite effect for turbine inlet pressure. This is because the pump power goes up more than the turbine power with increasing pressure. The decreasing MHD power carries directly over to specific impulse.

Figure 13 shows some internal effects of nonequilibrium on the conductivity and push power density. Conductivity is directly proportional to the nonequilibrium multiplier. Push power density is the force per unit volume, JxB, dotted with the velocity. It is

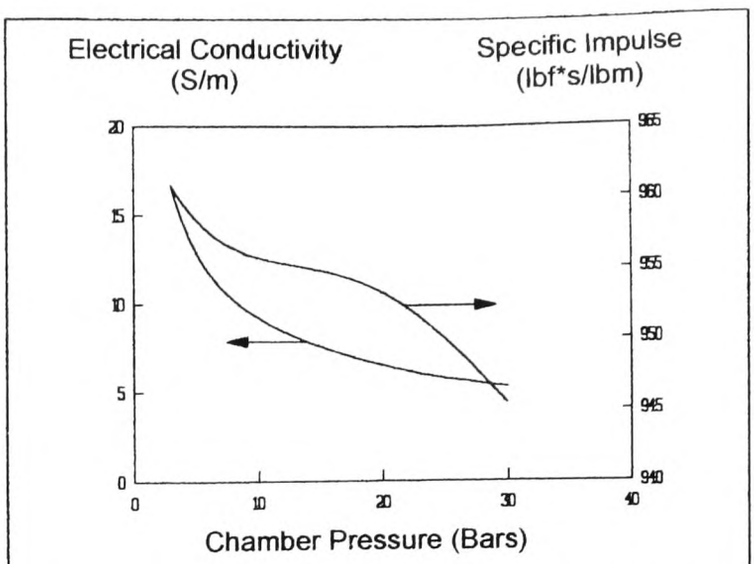

Figure 10. Effect of chamber pressure variation on electrical conductivity and specific impulse.

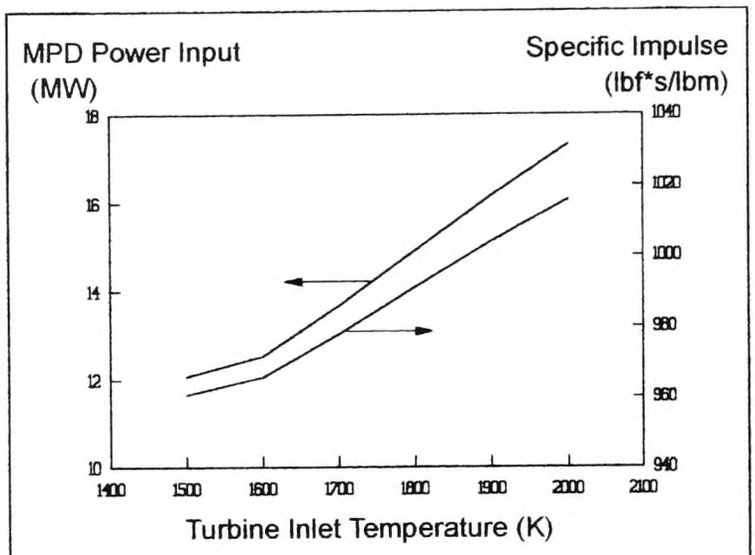

Figure 11. Turbine inlet temperature effect on the MHD power input and the specific impulse.

thus the actual mechanical power delivered to accelerate the plasma, as separate from the j^2/σ portion of the input power, which is converted to heat.

Figure 14 illustrates the effect of magnetic field on Hall parameter and push power. Note that neither the nonequilibrium multiplier nor the magnetic field effects the specific impulse, which is primarily determined by the MHD power input. They do, however, increase the power density attainable in the accelerator, thus allowing a more compact design.

Figure 15 shows the effect of load factor in the tradeoff between transverse and axial current density. A high value of J_y is desired to develop a push force, but as it is increased by increasing load factor, the parasitic J_x also increases in its absolute value. This increases the electrical dissipation. The best overall compromise seems to be a value of about 2 for load factor. This agrees with elementary theoretical considerations.

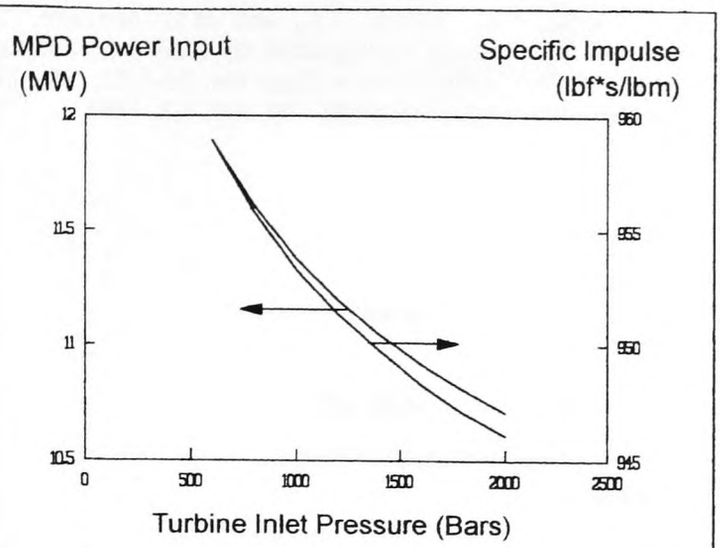

Figure 12. MHD power input and specific impulse verses turbine inlet pressure.

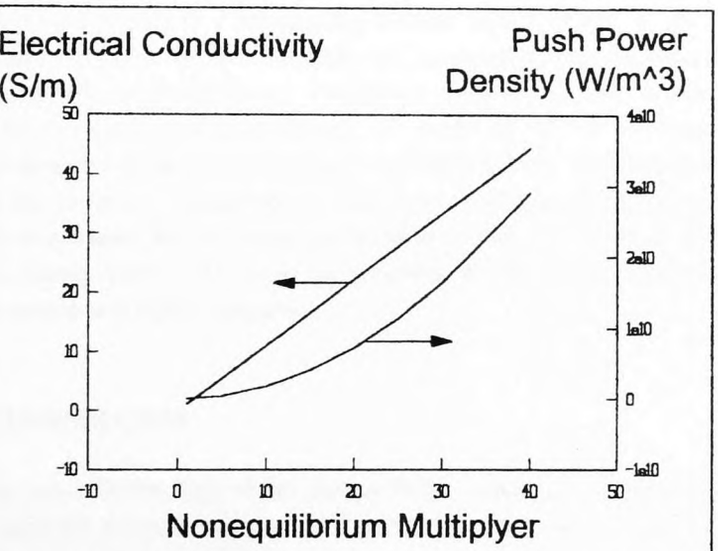

Figure 13. The combined nonequilibrium effect on electrical conductivity and push power density.

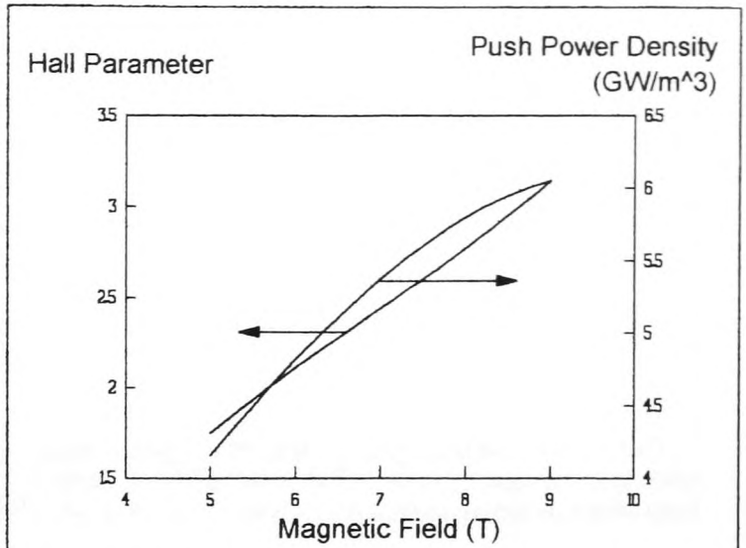

Figure 14. Magnetic field effect on Hall parameter and push power density.

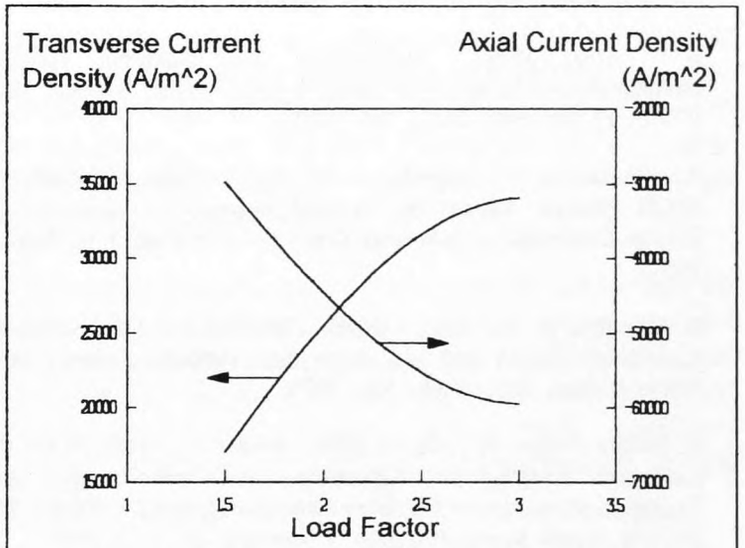

Figure 15. Load factor effect on transverse and axial current density.

Conclusions

Of the three key issues discussed earlier, none has been entirely resolved in this paper. The groundwork has, however, been laid for resolving the first issue, ie, is the performance improvement worth pursuing? This totally unoptimized design shows a specific impulse improvement of about 150 s over a comparable nuclear thermal rocket without MHD augmentation. The cost is that the mass of the rocket is approximately doubled by the mass of the magnet over that associated with a non-MHD nuclear thermal rocket.. Thus far no quantitative studies have been performed on the impact this would have on various missions, that is the next step in resolving the first key issue. Qualitative considerations indicate

that the MHD option would not be worthwhile for high earth orbit and trans-lunar missions, and perhaps not for Mars missions. But the MHD option definitely is worthwhile for asteroid belt and outer planet missions.

1. Cott, D.W., "An Integrated Nuclear MPD Thermal Rocket for Mars and Beyond," AIAA Paper No. 92-3584, 28th Joint Propulsion Conference and Exhibit, Nashville, TN, July 6-8, 1992.

2. Cott, D.W., Daniel, V.W., & R.A. Carrington, "Annular DC MHD Thrusters for Submarines," *Proceedings for the 27th Symposium on Engineering Aspects of MHD*, pp. 10.3-1 through 10.3-14, Reno, NV, June 27-29, 1989.

3. Cott, D.W., "Ionizational and Electron Thermal Nonequilibrium in MHD Boundary Layers," *AIAA Journal*, Vol. 9, No. 12, pp. 2404-2410, Dec 1971.

4. Watanabe, Y., Appelbaum, J., and I. Maya, "Stability of MHD Plasmas Ionized by Nuclear Fragments," *International Energy Conversion Engineering Conference*, Boston, MA, August 1991.

5.Vargaftik, N. B., *Tables on the Thermophysical Properties of Liquids and Gases*, 2nd Ed., Hemisphere Publishing Corp., John Wiley & Sons, New York, NY, 1975.

6. Svehla, Roger A., and McBride, Bonnie J., "FORTRAN IV Computer Program for Calculation of Thermodynamic and Transport Properties of Complex Chemical Systems," NASA TN D-7056, Lewis Research Center, Cleveland, OH, Jan 1973.

7. Gordon, Sanford, and McBride, Bonnie J., "Computer Program for Calculation of Complex Chemical Equilibrium Compositions, Rocket Performance, Incident and Reflected Shocks, and Chapman-Juoguet Detonations," NASA SP-273, Lewis Research Center, 1971.

8. Schwartz, J., Miller, J.R., and J.R.C. Williams, "TF Overall Current Density Scaling," National Magnet Laboratory, MIT, (Personal Communication of J.S. Herring, Idaho National Engineering Laboratory, subsequently communicated to Don Cott), original dated 11-7-88.

9. Thome, R.J., and J.M. Tarrh, *MHD and Fusion Magnets: Field and Force Design Concepts*, Wiley, 1982.

10. Parsley, R. C., Peery, S. D., Earley, S. M., Zubrin, R., Ramsthaler, J. H., and Ivanenok, J. F. III, "A Low Thrust Near Term Nuclear Thermal Rocket Concept," AIAA Paper No. 91-3352, 27th Joint Propulsion Conference, Sacramento, CA, July 6-8, 1991.

11. Clarke, J.S., Walton, J.T., and M.L. McGuire, "An Improved Heat Transfer Configuration for a Solid-Core Nuclear Thermal Rocket Engine," AIAA Paper No. 92-3583, 28th Joint Propulsion Conference, Nashville, TN, July 6-8, 1992.